AIP | Journal of Applied Physics

Electronic structure and optical absorption of the Bi4Ge3O12 and the Bi4Si3O12 scintillators in ultraviolet region: An ab initio study

A. F. Lima, S. O. Souza, and M. V. Lalić

Citation: J. Appl. Phys. 106, 013715 (2009); doi: 10.1063/1.3160291
View online: http://dx.doi.org/10.1063/1.3160291
View Table of Contents: http://jap.aip.org/resource/1/JAPIAU/v106/i1
Published by the AIP Publishing LLC.

Electronic structure and optical absorption of the $Bi_4Ge_3O_{12}$ and the $Bi_4Si_3O_{12}$ scintillators in ultraviolet region: An *ab initio* study

A. F. Lima, S. O. Souza, and M. V. Lalić[a)]
Departamento de Física, Universidade Federal de Sergipe, P. O. Box 353, São Cristóvão, Sergipe 49100-000, Brazil

(Received 5 March 2009; accepted 8 June 2009; published online 10 July 2009)

Ab initio calculations based on density-functional theory have been employed to study structural and electronic properties of $Bi_4Ge_3O_{12}$ (BGO) and $Bi_4Si_3O_{12}$ (BSO), as well as their optical characteristics in ultraviolet region, up to 40 eV. The electronic structure around the band gap is found to be similar in both compounds, dominated by the O *p*- and the Bi *s*-states (valence band top) and the Bi *p*-states (conduction band bottom). The gap is found to be indirect in both BGO and BSO. The optical spectra are analyzed, compared, and interpreted in terms of calculated band structures. It is shown that the absorption process involves significant energy flow from the O ions to the Bi ions. This fact stresses importance of the first neighborhood of the Bi (six O's forming an octahedron), which is more distorted in the BSO than in the BGO. The latter difference is mainly responsible for the different absorption characteristics of the BGO and BSO. © *2009 American Institute of Physics*. [DOI: 10.1063/1.3160291]

I. INTRODUCTION

Scintillators are materials that convert energy of incident radiation into emission of light. They are utilized as detectors in scientific research, industry, and medicine. Their working principle is generally understood in terms of basic quantum mechanics: The incident radiation excites the atoms and creates electron-hole pairs whose energy is then transferred to some luminescent center. By returning to its ground state the latter emits radiation in a visible or near ultraviolet range, which is then captured and quantified by output electronics. Thus, in order to understand a scintillation process in any specific material the following aspects should be studied: (1) How the material absorbs the incident radiation? (2) How the absorbed energy is transferred to the luminescent centers? (3) How the luminescent centers emit the radiation? In this paper we pretend to discuss and clarify the first two aspects of scintillation process in the bismuth orthogermanate $Bi_4Ge_3O_{12}$ (BGO) and the bismuth orthosilicate $Bi_4Si_3O_{12}$ (BSO), when the incident radiation energy ranges from 0 to 40 eV.

The BGO, discovered in 1973 by Weber and Monchamp,[1] is a famous scintillator owing to its remarkable characteristics such as high density, large light output, large hardness, and low afterglow.[2,3] It is utilized in the largest electromagnetic calorimeter in the world at CERN, Geneva, and widely applied in nonlinear optical devices and nuclear medicine.[4–6] The BSO crystallizes into the same structure as the BGO, and resembles him in many aspects. It, however, has faster response (three times) but smaller light output (five times) then BGO.[7] For this reason, the BGO and BSO are considered as complementary scintillators: The BGO is preferably used for some applications and BSO for others.[8]

There are many published experimental studies about the BGO, and much less about the BSO (its commercial use started more recently). Both materials are intrinsic scintillators: Their luminescent centers are the Bi ions whose emission is due to $^3P_1 \rightarrow {}^1S_0$ electronic transitions[1] (conclusion is drawn for the BGO, but there is no reason to be different for the BSO). The optical absorption of the pure BGO in the ultraviolet region was analyzed by Antonangeli *et al.*[9] via measurement of its reflectivity spectrum. The authors discussed and interpreted the measured spectra in terms of the energy band diagram constructed with the aid of cluster calculations[10,11] which took into account just the first neighborhood of the Bi and the Ge ions within the BGO crystal lattice. The Rivas and Berrondo[12] reported an *ab initio* Hartree–Fock computation of the BGO and BSO absorption and emission energies, but again considering just a small cluster of atoms around the Bi, and not a full crystal structure.

In this paper we present the first-principles calculations of the structural, electronic and some optical properties of the BGO and BSO, taking into account their complete crystal structures. To our knowledge it is the first time that this kind of treatment is applied to these compounds. Our objective is twofold: (1) to determine microscopic properties of each compound separately (confronting the calculations with the experimental data whenever possible), and (2) to compare these properties trying to discover why the two materials exhibit different scintillation characteristics. Toward these goals we analyzed and compared the electronic structures of both compounds, and on this basis determined their complex dielectric tensors, being able to identify the electronic transitions responsible for the optical absorption. We also calculated optical constants as functions of incident radiation energy up to 40 eV (far ultraviolet region). All calculations were performed with the spin-orbit (SO) interaction taken into account. Analysis of obtained results enabled us to clarify the process of optical absorption and energy transfer to the luminescent centers in the BGO and BSO, as well as to discuss the possible origin of their different luminescent characteristics. Some preliminary results of actual research

[a)]Electronic mail: mlalic@fisica.ufs.br.

have been published recently,[13] but employing less precise calculations (electronic and optical properties were calculated for photon energies from 0 to 25 eV), without taking into account the SO coupling and without any comparison with the experimental data. Here is presented a complete study, which overcomes the mentioned deficiencies.

II. CALCULATION DETAILS

The self-consistent calculations of pure BGO and BSO compounds were performed by density-functional theory[14] (DFT) based, full potential linear augmented plane wave (FP-LAPW) method[15] as embodied in WIEN2K computer code.[16] In this method, the electronic wave functions, charge density, and crystal potential are expanded in spherical harmonics inside the nonoverlapping spheres centered at each nuclear position (atomic, or muffin-tin (MT) spheres with radii R_{MT}), and in plane waves in the rest of the space (interstitial region). The choice for the atomic sphere radii R_{MT} (in atomic units) was 2.3 for Bi, 1.8 for Ge, and 1.45 for O (BGO), and 2.3 for Bi, 1.6 for Si, and 1.4 for O (BSO). Inside atomic spheres the partial waves were expanded up to $l_{\max}=10$, while the number of plane waves in the interstitial was limited by the cutoff at $K_{\max}=7.0/R_{\mathrm{MT}}$. The augmented plane wave basis set was utilized in both cases. The charge density was Fourier expanded up to $G_{\max}=14$. A mesh of six k-points in the irreducible part of the Brillouin zone was used. Exchange and correlation effects were treated by generalized-gradient approximation (GGA96).[17] The Bi $5d$, $6s$, $6p$, the O $2s$, $2p$, the Ge $3d$, $4s$, $4p$, and the Si $2p$, $3s$, and $3p$ electronic states were considered as valence ones, and treated within the scalar-relativistic approach, whereas the core states were relaxed in a fully relativistic manner. Two kinds of calculations were performed for both systems. In the first one the SO coupling has not been taken into account, while in the second one the SO coupling has been switched on for the Bi and the Ge atoms. In the second case, the 2374 partial waves constituted the second variational basis set inside the MT spheres. This approach permitted us to estimate the importance of the effects of the SO interaction on calculated properties.

The calculations were performed in the following sequence. First, the crystalline structures of both BGO and BSO were computationally optimized by determining the equilibrium lattice constants and the atomic positions within the each unit cell. Second, the electronic structure for both compounds was calculated using a mesh of six k-points in the irreducible part of the Brillouin zone. Finally, the optical characteristics were analyzed by calculating the complex dielectric tensor ε, whose imaginary part $\mathrm{Im}(\varepsilon)$ is directly proportional to the optical absorption spectrum of the materials. The $\mathrm{Im}(\varepsilon)$ is computed within the frame of random phase approximation, in the limit of linear optics and neglecting electron polarization effects, using the following formula:[18]

$$\mathrm{Im}\,\varepsilon_{\alpha\beta}(\omega)=\frac{4\pi^2e^2}{m^2\omega^2}\sum_{i,f}\int_{BZ}\frac{2dk}{(2\pi)^3}|\langle\varphi_{fk}|P_\beta|\varphi_{ik}\rangle| \times|\langle\varphi_{fk}|P_\alpha|\varphi_{ik}\rangle|\cdot\delta(E_f(k)-E_i(k)-\hbar\omega) \quad (1)$$

for a vertical transition from a filled initial state $|\varphi_{ik}\rangle$ of energy $E_i(k)$ to an empty final state $|\varphi_{fk}\rangle$ of energy $E_f(k)$ with the same wave vector k. ω is the frequency of the incident radiation, m is the electron mass, P is the momentum operator, and α and β stand for projections x,y,z.

On the basis of calculated electronic structure (i.e., the Kohn–Sham orbitals $|\varphi_{ik}\rangle$) of the BGO and BSO we computed the $\mathrm{Im}(\varepsilon)$ for both compounds up to incident radiation energy of $\hbar\omega=40$ eV. The real part of dielectric tensor is then determined using Kramers–Kronig relation. Both real and imaginary parts of ε were calculated with a mesh of 44 k-points in the irreducible wedge of the first Brillouin zone in the case when the SO coupling was off and 55 k-points when the SO coupling was switched on. Owing to cubic symmetry the dielectric tensor is diagonal, with $\varepsilon_{xx}=\varepsilon_{yy}=\varepsilon_{zz}=\varepsilon$. It is thus reduced to a scalar function $\varepsilon(\omega)$. The BGO spectrum was adjusted to match the experimental gap (4.96 eV) as found by Antonangeli *et al.*[9] by raising the conduction band position in energy by "scissors operator," while the BSO spectrum was not energy shifted.

III. RESULTS AND DISCUSSIONS

A. Computational optimization of the crystal structure

The BGO and BSO crystallize in cubic symmetry, space group I-43d, where the Bi, Ge (or Si), and O atoms occupy 16c, 12a, and 48e positions, respectively, according to Wyckoff's notation. Primitive unit cell contains two formula units and does not have a center of inversion. Each Bi ion is surrounded by six oxygens arranged in a strongly distorted octahedron: Three of them are situated nearer to the Bi than the other three. The Ge (or Si) atoms are surrounded by four oxygens, all at the same distance, arranged in a perfect tetrahedron.

The computational relaxation of the lattice parameters resulted in $a=10.594$ Å for the BGO, and $a=10.379$ Å for the BSO (Ref. 13), the values that correspond to the 2% (BGO) and 3% (BSO) larger unit cell volumes than the experimental ones.[19,20] All atomic positions inside these unit cells were then optimized using the damped Newton scheme, until the forces acting on each atom became less than 5.0 mRy/a.u.

The calculated interatomic distances between the Bi, Ge, and Si atoms on one side, and their nearest-neighbor oxygens on the other, are shown in Table I. They compare well with the experimental data, obtained at the ambient temperature.[21,22] By comparing these distances, one can notice that the three nearest O's are closer to the Bi in the BSO than in the BGO. At the same time the three second-nearest O's are situated farther from the Bi in the BSO than in BGO. Therefore, the octahedron of oxygens around the Bi is more distorted in the BSO than in the BGO. This fact could be important to explain the different scintillation properties of these two materials, as will be discussed in the Sec. III C.

TABLE I. Calculated equilibrium interatomic distances (Å) in BGO and BSO, compared to the experimental data. First coordination sphere of Bi consists of three nearest and three second-nearest oxygens. Coordination of the Ge (Si) is regular: All four nearest-neighbor oxygens are situated at the same distance.

	BGO			BSO	
	Theory (this work)	Expt.[a]		Theory (this work)	Expt.[b]
Bi–O	2.221(3)	2.149(3)	Bi–O	2.212(3)	2.189(3)
	2.584(3)	2.620(3)		2.595(3)	2.598(3)
Ge–O	1.782(4)	1.736(4)	Si–O	1.649(4)	1.613(4)

[a]Reference 21.
[b]Reference 22.

Another conclusion is that the tetrahedron of O's around the Si in BSO is more compact than the corresponding tetrahedron around the Ge in the BGO (nearest O's are situated closer to the Si in BSO).

B. Electronic structure

Figure 1 presents the calculated electronic structure of the BGO and BSO without taking into account the SO coupling. Band gap in the BGO is calculated to be 3.54 eV, and in the BSO 4.04 eV. The experimental values for these gaps were estimated from the optical absorption thresholds: 4.13 eV for the BGO (Ref. 23), and 4.34 eV for the BSO (Ref. 24). These values, however, refer to the energy difference between the top of the valence band and the exciton level with lowest energy. Thus, the real gaps, expressing the energy difference between the valence band top and the conduction band bottom, should be larger than reported. Antonangeli *et al.*[9] determined the BGO band gap as 4.96 eV extracting the excitonic transitions from the absorption spectra. In any case, our calculations underestimated the BGO and BSO gaps due to a well known effect of the GGA approximation implemented in the DFT. Figure 1 reveals a similarity of the electronic density of states (DOS) in two

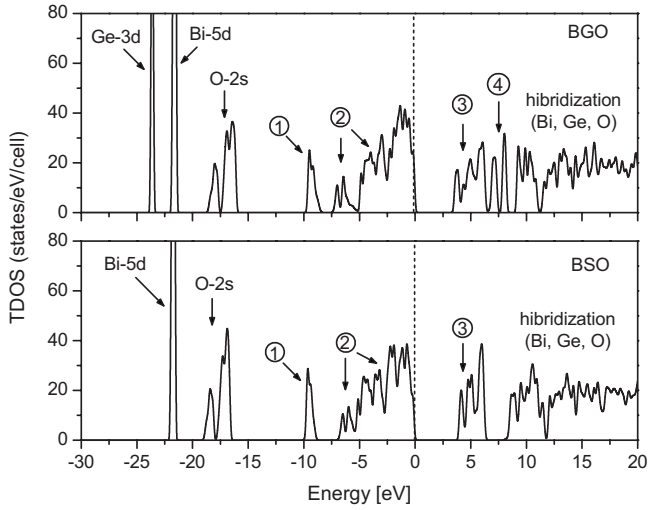

FIG. 1. Calculated total DOS of the BGO and BSO scintillators, with the SO interaction neglected. Predominant orbital characters of some bands are indicated. Dashed line indicates Fermi level.

TABLE II. Population analysis of each of the four DOS blocks shown in Fig. 1 for both BGO and BSO. First column shows the number of electrons accommodated in each block, counted per atom, and confined within the corresponding atomic sphere. Second column shows the predominant orbital character of these electrons.

	BGO		BSO	
Block	Number of electrons per atom	l -type	Number of electrons per atom	l -type
1	Bi: 0.90	s	Bi: 0.91	s
	Ge: 0.09	s,p	Si: 0.36	s,p
	O: 0.11	p	O: 0.11	p
2	Bi: 0.99	s,p	Bi: 0.99	s,p
	Ge: 0.90	s,p	Si: 0.67	s,p
	O: 3.20	p	O: 3.13	p
3	Bi: 1.51	p	Bi: 1.70	p
	Ge: 0.30	s	Si: 0.12	s
	O: 0.46	s,p	O: 0.41	s,p
4	Bi: 0.26	p	⋯	⋯
	Ge: 0.51	s,p		
	O: 0.29	s,p		

compounds, especially within a valence region. The major difference is found at the conduction band bottom which is compact in the BGO, while in the BSO exists one block which is isolated from the rest of the conduction band. The Bi and Ge d-states are completely populated and localized (with almost no dispersion), while the O $2s$-states exhibit some dispersion but they lay in low-energy region. These states can be characterized as semicore ones. The true valence region begins at the energy of -0.4 Ry, and consists of the mixture of the Bi, Ge(Si) and O s- and p-states. In order to determine predominant atomic and orbital character of electronic states in this region and at the conduction band bottom, we divided them into four blocks and performed a population analysis of the latter, which is presented in Table II.

An analysis of atomic and l-character of each block (Fig. 1 and Table II) yields the similar conclusions for both compounds. Block 1 is by far dominated by the Bi $6s$-states. Block 2 consists of the s- and p-states of all the constituents, but is dominated by the O $2p$-states. Within the block 3 the Bi p-states are clearly dominant in the case of the BSO, while in the BGO exists a non-neglecting amount of the Ge s-states and the O p-states. Block 4, positioned within the BGO conduction band, is dominated by the Ge p-states, with some Ge s-states present as well. A corresponding block does not exist in the BSO spectrum owing to absence of the Si-states in this energy range. The upper part of conduction region consists of a mixture of many states and cannot be attributed to any particular state of any particular atom.

Inclusion of the SO interaction introduces some differences in the BGO and BSO electronic structures, as shown in Fig. 2. The principal changes occurred in the low-energy part of the DOS where the Bi $5d$- and Ge $4d$-states are split into the $j=3/2$ and $j=5/2$ components. Another change is per-

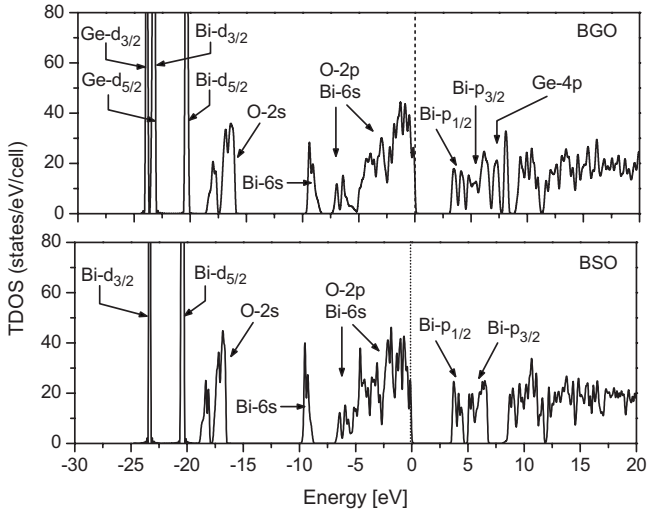

FIG. 2. Calculated total DOS of the BGO and the BSO, with the SO interaction switched on. Predominant orbital characters of bands are indicated. Dashed line indicates Fermi level.

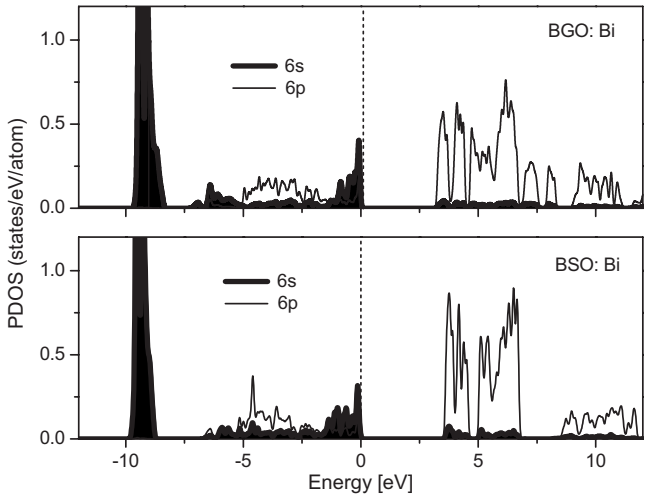

FIG. 4. Calculated partial DOS of the Bi atom within the BGO and the BSO compounds. Dashed line indicates Fermi level.

ceived at the conduction band bottom where the Bi $6p$-states split into the $j=1/2$ and $j=3/2$ components. This splitting diminishes the calculated band gap values to 3.19 eV for the BGO and 3.90 eV for the BSO. The rest of the DOS spectrum is not altered in comparison with the DOS presented in Fig. 1. The population analysis presented in Table II stays essentially the same. The splitting between the Bi $5d$ components in the BGO is found to be approximately 3.0 eV, in good agreement with the conclusion of Antonangeli *et al.*[9] who estimated this splitting as 2.8 ± 0.1 eV. The Bi $6p$ components in the BGO are split approximately 1.97 eV, while Antonangeli *et al.*[9] determined this splitting as 1.8 ± 0.1 eV. In the case of the BSO the splitting between the Bi $5d$ and the Bi $6p$ components are calculated to be 2.91 and 1.87 eV, respectively, very similar to the case of the BGO. The Bi $6p_{1/2}$- and $6p_{3/2}$-states, however, are fully separated, while in the BGO this does not happen.

The structure of electronic bands of the BGO and the BSO in vicinity of the fundamental gap is shown in Fig. 3. In the conduction region the BGO and BSO bands exhibit different shape along every line except the line H–N. The band

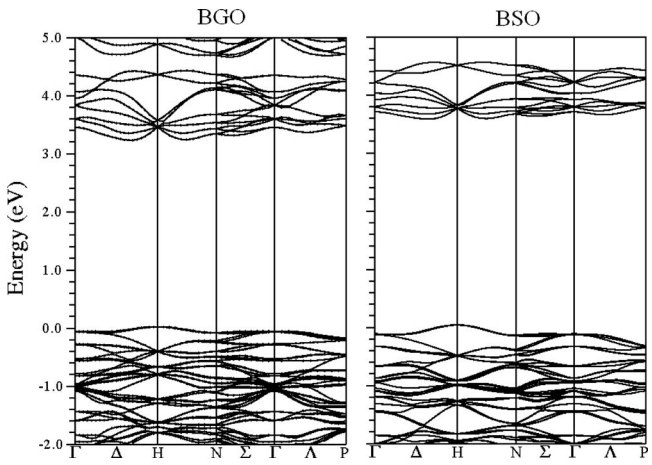

FIG. 3. Electronic band structure in the vicinity of fundamental gap: BGO (left) and BSO (right). SO coupling has been included in calculations.

structures at the top of the valence region are quite similar. For both BGO and BSO the energy maximum of the valence band occurs at the H point, while the energy minimum of the conduction band occurs in the vicinity of the Δ point along the line Γ-H. Thus, our calculations predict the indirect band gap for both BGO and BSO.

The results of the DFT calculations for the BGO, presented in Fig. 2, generally support the energy band diagram deduced by Antonangeli *et al.*,[9] but also reveal some important differences.

(1) Antonangeli *et al.* considered the populated O $2p$-states split into the two separate bands (bonding σ- and shortest O–O π-states). This conclusion was supported by theoretical investigation of the $(GeO_4)^{4-}$ cluster performed by Hojer *et al.*[10] According to our DFT calculations, all populated O $2p$-states are concentrated in one single band.

(2) Antonangeli *et al.* considered that the populated Bi $6s$-states form a very top of the valence band (being all concentrated there). They drew this conclusion on the basis of the paper of the Moncorgé *et al.*[11] who calculated energy levels of the $(BiO_6)^{9-}$ cluster. The DFT calculations split the Bi $6s$-states off (Fig. 4) owing to their mutual interaction. Bonding $6s$-states are localized and situated in the separated band centered at −9 eV (block 1 in Fig. 1), accommodating approximately one electron (Table II). Antibonding $6s$-states are delocalized (due to hybridization with the O $2p$-states), with the energy dispersed from −7 to 0 eV (block 2 in Fig. 1), accommodating another one electron (Table II). Although exists a peak of the Bi $6s$ DOS located at the Fermi level, these states cannot be considered as being dominant there in comparison with the O $2p$-states.

(3) In the energy diagram of Antonangeli *et al.*[9] the energies of the Bi $5d$ and the O $2s$-states overlap. The DFT calculations clearly separate these states positioning the energy of the Bi $5d$-states below the energy of the O $2s$-states.

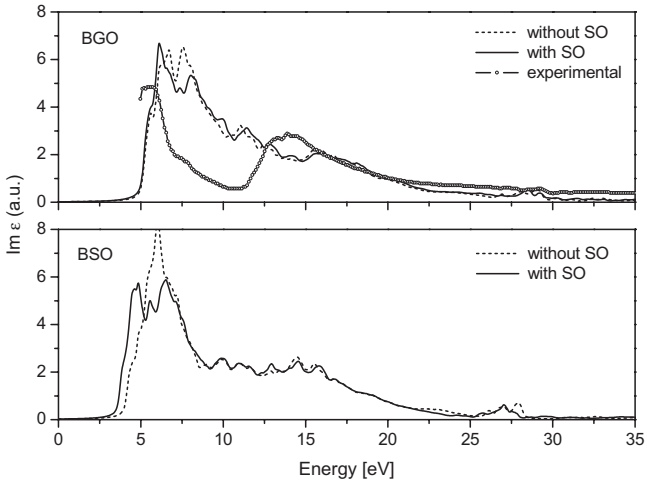

FIG. 5. Imaginary part of dielectric function for the BGO (top) and the BSO (bottom) as a function of energy of incident radiation. It is directly proportional to optical absorption spectra of the materials. The absorption of the BGO is compared to the experimental curve (Ref. 9) from which the excitonic peak below 5 eV has been omitted.

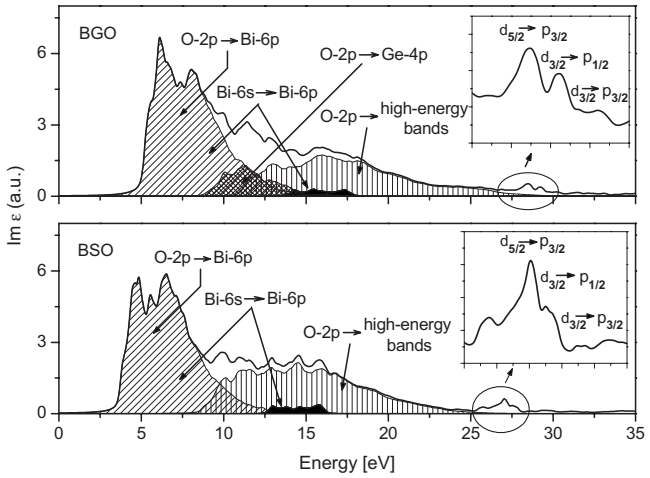

FIG. 6. Imaginary part of dielectric function for the BGO (top) and the BSO (bottom) as a function of incident radiation energy, and interpreted in terms of calculated band structure. Electronic transitions between O p- and the Bi p-states dominate the spectrum in both compounds.

C. Optical properties

The imaginary part of dielectric function Im(ε), directly proportional to absorption spectrum, is shown in Fig. 5 for both BGO and BSO, and for both types of calculations (with and without SO). In the case of the BGO it is also presented the experimental curve determined by Antonangeli *et al.*,[9] from which was extracted the lowest energy peak with excitonic nature.

Both absorption spectra can be roughly divided into three distinct structures: (1) the low-energy one (from 5 to 11 eV for the BGO, and from 4 to 9 eV for the BSO), characterized by the highest intensity; (2) the middle-energy one (from 11 to 20 eV for the BGO and from 9 to 20 eV for the BSO) with medium intensity; and (3) the high-energy one, positioned above the 25 eV for both compounds. The experimental BGO curve also roughly follows the same pattern. The theoretical BGO middle-energy structure is, however, less pronounced and intense. The SO interaction essentially influences only low- and high-energy structures, while the main features of the middle-energy structure are already reproduced by the non-SO calculations. The reason for this is the SO splitting of the Bi 6p- and the 5d-states since the electronic transitions that involve these states are characterized by the lowest and the highest absorption energies.

Observing Fig. 5 one can notice different forms of absorption curves for the BGO and the BSO. The fine structure of the low-energy peaks is different, as well as the position of the high-energy peaks. The difference is observed within the middle-energy structure as well. In the case of the BGO this structure is more intense in its lower energy part, while in the case of the BSO it is essentially flat.

An interpretation of the BGO and BSO absorption spectra in terms of their electronic structures, presented at Fig. 6, reveals the manner by which the compounds absorb incident radiation. The largest part of absorption for both compounds, described by the low-energy structure of the spectrum, is caused by electronic transitions from the band at the top of the valence region (block 2 at Fig. 1 and Table II) to the conduction band bottom (block 3 at Fig. 1 and Table II). It is thus generated by transitions from the O 2p-states to the Bi 6p-states, and from the antibonding Bi 6s- to the Bi 6p-states. The middle-energy structure is generated by the electronic transitions from the same band to the empty bands with higher energies (hybridization bands), and from the single band centered at −9 eV (block 1 at Fig. 1 and Table II) to the conduction band bottom (block 2 at Fig. 1 and Table II). Therefore, this part of the spectrum is dominated by transitions from the populated O 2p-states to the other O or Ge empty states with high energy. The transitions from the bonding Bi 6s- to the empty Bi 6p-states contribute very little to absorption. In the case of the BGO there are additional transitions from the valence band top (block 2) to the empty band centered around 7.5 eV (block 4 at Fig. 1 and Table II), i.e., from the O 2p-states to the Ge 4p-states. These transitions elevate the intensity of the BGO absorption between 10 and 13 eV approximately. In the case of the BSO the corresponding transitions from the O 2p- to the Si 3p-states are missing, making a difference in the middle-energy part of the absorption spectrum between two compounds. Finally, the third structure in the BGO and the BSO absorption spectra, situated between 28 and 30 eV for the BGO and between 25 and 28 eV for the BSO, is dominated by the transitions from the occupied Bi 5d-states to the empty Bi 6p-states, as shown at Fig. 6.

The calculated optical absorption spectra (Fig. 6), together with the characterization of the electronic structures (Figs. 2 and 4, Table II), permit a better understanding of basic scintillation characteristics of the BGO and BSO, namely, how they absorb the energy of incident radiation and how this energy is transferred to the luminescent centers. Since the intensity of absorption depends on quantity of the occupied and empty electronic states at disposal for each electronic transition, we conclude that the major part of incident energy is not directly absorbed by the Bi atoms (via 6s to 6p transitions). The O 2p-states are clearly dominant within the highest energy band in the valence region, thus the

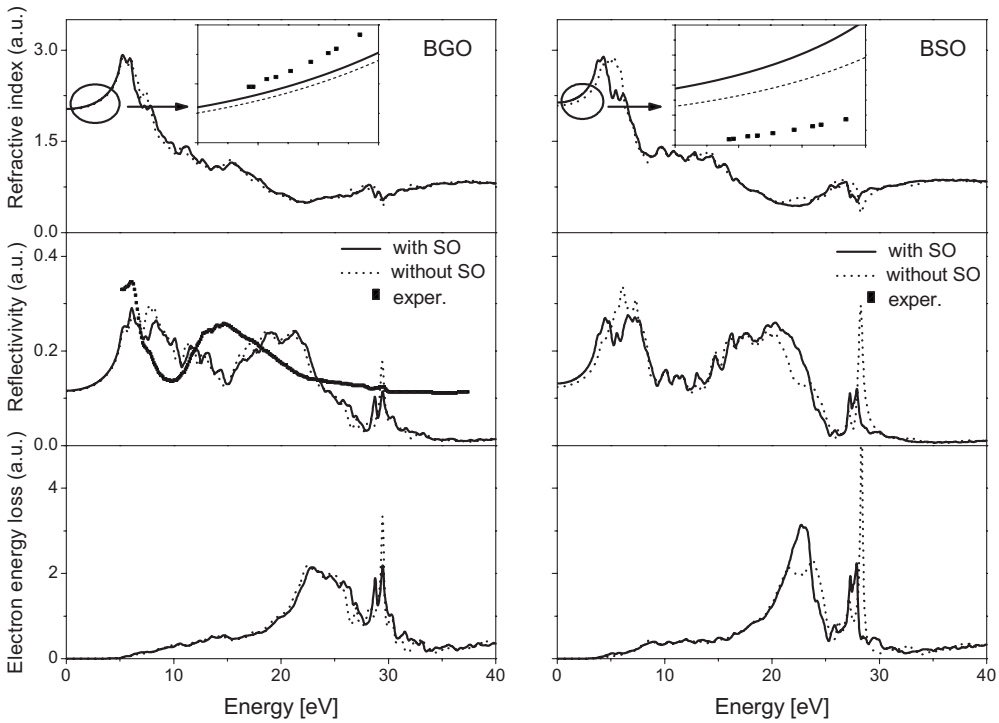

FIG. 7. Refractive index, reflectivity, and electron energy loss for the BGO (left) and the BSO (right) compounds, as calculated by the FP-LAPW method. The experimental data shown at the offsets of the top figures have been taken from Ref. 25. The reflectivity of the BGO is compared to the experimental data (Ref. 9) from which the excitonic peak below 5 eV has been omitted.

O atoms around the Bi absorb the largest part of the energy by their *p*-electrons, and transfer it to the Bi atoms (in this process the *p*-electrons are transferred from the O to the Bi). By this way the Bi ions receive the energy that turns them to the excited state. Their return to the ground state defines the emission spectrum of the compounds, but this process is not analyzed here since the present calculation method does not describe adequately the excited states in solids. We can, however, discuss this process briefly on the basis of the presented results.

The differences that exist between the BGO and BSO electronic structures and optical absorption spectra are mainly caused by (1) the presence of different atoms in the compounds (Ge or Si), and (2) the different arrangements of O's around the Bi. Since our electronic structure results demonstrate that the BGO and the BSO bands in the vicinity of the Fermi level are dominated by the Bi *s*- and *p*- and the O *p*-states, while the Ge- and Si-states play a secondary role, we attribute a major part of these differences to the second cause. The fact that the absorbed energy flows from the O's to the Bi enforces the conclusion that the different absorptions of the BGO and BSO originate mainly from the different arrangement of the nearest O's around the Bi.

The emission characteristics of the BGO and the BSO mainly depend on the Stokes shift of the Bi nucleus and the accommodation of its electronic system to this movement (a fact which defines the excitation state of the Bi atom in both compounds). Therefore, these characteristics should also strongly depend on the Bi nearest surrounding since the latter exerts the major influence on the Bi atom. If these surroundings in the BGO and the BSO were equal, then the Bi nuclei would recoil in the approximately same manner in both compounds, the Bi electrons would relax similarly, and the excited states of the Bi in two compounds would not be too different. In this case, we should expect similar emission properties of the BGO and the BSO. Thus, the different arrangements of the nearest O's around the Bi certainly play a very important role in explaining the different emission spectra of the BGO and the BSO.

Knowing the complex dielectric function ε one can calculate various optical constants which characterize the propagation of the electromagnetic wave through the material.[18] Figure 7 displays the variation of the refractive index, the reflectivity, and the electron energy loss of the BGO and BSO as functions of incident radiation energy, calculated by the FP-LAPW method. It is seen that the refraction indices for both BGO and BSO reach maximal values for the energies near the absorption thresholds of the materials (band gap energies). For higher energies they exhibit decreasing tendency, somewhat steeper for the BGO than for the BSO. The calculated refractive indices compare well with the existing experimental data recorded in the low-energy part of the spectra, which is shown in the offsets at the first panel of Fig. 7. The calculated values of the static (zero frequency) dielectric constants are found to be 2.08 (BGO) and 2.23 (BSO), not very far from the experimental estimative[25] (2.09 for the BGO and 2.02 for the BSO). The reflectivity spectra can be roughly characterized by three broad peaks (structures), similar to the case of the absorption spectra. In the case of the BGO, the calculated spectrum is compared to the experimental one (Ref. 9), and we find that these two fairly agree. The principal disagreement is in the position of the calculated second peak which is found to be centralized around 20 eV, while the corresponding experimental peak is localized around the 15 eV. This discrepancy is probably caused by shortcomings of the DFT when de-

scribing the conduction region in materials. The electron energy-loss spectra (EELS) determine a probability that the fast electrons, traversing through the materials, loose energy per unit length. According to our calculations, there are three prominent features at these spectra: one very broad peak centralized around the energy of the 23–24 eV in both compounds, and two sharp, closely spaced peaks at somewhat higher energies (28.7 and 29.5 eV for the BGO, and 28.7 and 29.6 eV for the BSO). These peaks are usually interpreted as plasmon peaks, which denote the energies at which the electronic charge in crystal performs collective oscillations.

Finally, Figs. 5 and 7 confirm an important role of the SO coupling in describing the optical characteristics of the BGO and the BSO. The splitting of the Bi 6*p*-states significantly changes the lowest energy part of optical spectra, while the splitting of the Bi 5*d*-states influences the highest energy part of these spectra. The SO coupling is especially important for describing reflectivity and EELS spectra, at which it divides the highest energy peak into two (BGO and BSO) and even dislocates them in position (BSO), as shown in Fig. 7.

IV. CONCLUSIONS

We performed an *ab initio* theoretical study of the BGO and BSO scintillators using DFT based FP-LAPW method. Our objective was to investigate structural, electronic and optical properties of these materials in the ultraviolet region (up to 40 eV).

Our principal conclusions are the following.

- The principle effect of substitution of Ge (BGO) for Si (BSO) is the change in interatomic distances between the Bi and its nearest-neighbor oxygens: octahedral environment around the Bi is more distorted in the BSO than in the BGO.
- Band structures of the BGO and the BSO are similar, exhibiting a major difference at the conduction band bottom (different arrangement of empty bands); band gaps in both compounds are indirect.
- The top of the valence band in both compounds is dominated by the O *p*-states and the bottom of the conduction band by the Bi *p*-states. The Bi 6*s*-states are split due to mutual interaction. The bonding 6*s*-states are concentrated at the single band localized approximately 9 eV below the Fermi level while the antibonding ones are dispersed over the broad band at the top of the valence region.
- The optical absorption spectra for both BGO and BSO can be roughly characterized by three prominent features (peaks). The low-energy one, which exhibits the maximal intensity, originates from the antibonding Bi $6s \rightarrow$ Bi $6p$ and the O $2p \rightarrow$ Bi $6p$ transitions, the second being dominant one.
- The O atoms around the Bi absorb the largest part of incident radiation energy. This energy is transferred to the luminescent center, Bi, and turns it to the excited state. The absorption and the emission characteristics thus depend crucially on the oxygen arrangement around the Bi.
- The SO interaction influences the BGO and the BSO DOS spectra mostly in the low-energy part of the valence region and at the bottom of the conduction band, where it splits the Bi 5*d*- and 6*p*-states, respectively. These splitting affect the optical spectra, changing significantly their low-energy and high-energy features.
- Our theoretical results for optical characteristics compare well with the existing experimental data (available mostly for the BGO). The calculated electronic structure of the BGO confirms the basic features of the energy band diagram constructed earlier on the basis of the reflectivity spectra, but also reveals some important differences, mostly related to the Bi 6*s*-states.

ACKNOWLEDGMENTS

The authors gratefully acknowledge the CNPq and FAPITEC-SE (Brazilian funding agencies) for financial support.

[1] M. J. Weber and R. R. Monchamp, J. Appl. Phys. **44**, 5495 (1973).
[2] L. Dimesso, G. Gnappi, and A. Montenero, J. Mater. Sci. **26**, 4215 (1991).
[3] L. Kóvacs, S. G. Raymond, B. J. Luff, A. Péter, and P. D. Townsend, J. Lumin. **60-61**, 574 (1994).
[4] G. Blasse, Chem. Mater. **6**, 1465 (1994).
[5] P. Lecoq, J. Lumin. **60-61**, 948 (1994).
[6] R. Akhmetshin, M. Z. Wang, R. S. Guo, H. C. Huang, R. S. Lu, K. L. Tsai, K. Ueno, C. H. Wang, F. I. Chou, Y. Y. Wei, and W. S. Hou, Nucl. Instrum. Methods Phys. Res. A **455**, 324 (2000).
[7] M. Kobayashi, M. Ishii, K. Harada, and I. Yamaga, Nucl. Instrum. Methods Phys. Res. A **372**, 45 (1996).
[8] V. Vaithianathan, P. Santhanaraghavan, P. Ramasamy, L. Righi, and G. Bocelli, Mater. Chem. Phys. **78**, 1 (2003).
[9] F. Antonangeli, N. Zema, and M. Piacentini, Phys. Rev. B **37**, 9036 (1988).
[10] G. Hojer, S. Meza-Hojer, and G. Hernandez de Pedrero, Chem. Phys. Lett. **37**, 301 (1976).
[11] R. Moncorgé, B. Jacquier, G. Boulon, F. Gaume-Mahn, and J. Janin, J. Lumin. **12-13**, 467 (1976).
[12] J. F. Rivas-Silva and M. Berrondo, J. Phys. Chem. Solids **59**, 1627 (1998).
[13] M. V. Lalic and S. O. Souza, Opt. Mater. (Amsterdam, Neth.) **30**, 1189 (2008).
[14] P. Hohenberg and W. Kohn, Phys. Rev. **136**, B864 (1964); W. Kohn and L. J. Sham, *ibid.* **140**, A1133 (1965).
[15] O. K. Andersen, Phys. Rev. B **12**, 3060 (1975); D. J. Singh, *Plane Waves, Pseudopotentials and the LAPW Method* (Kluwer Academic, Dodrecht, 1994).
[16] P. Blaha, K. Schwarz, G. K. H. Madsen, D. Kvasnicka, and J. Luitz, *WIEN2k, an Augmented Plane Wave+Local Orbitals Program for Calculating Crystal Properties* (Karlheinz Schwarz, Techn Universität, Wien, Austria, 2001).
[17] J. P. Perdew, S. Burke, and M. Ernzerhof, Phys. Rev. Lett. **77**, 3865 (1996).
[18] W. D. Lynch, *Handbook of Optical Constants of Solids*, edited by E. D. Paik (Academic Press, New York, 1985).
[19] F. Radaev, L. A. Muradyan, F. Kargin Yu, V. A. Sarin, V. N. Kanepit and V. I. Simonov, Kristallografiya **35**, 361 (1990).
[20] J. Barbier, J. E. Greedan, T. Asaro, and G. J. McCarthy, Eur. J. Solid State Inorg. Chem. **27**, 855 (1990).
[21] P. Fischer and F. Waldner, Solid State Commun. **44**, 657 (1982).
[22] H. Liu and C. Kuo, Z. Kristallogr. **212**, 48 (1997).
[23] P. Kozma and P. J. Kozma, Nucl. Instrum. Methods Phys. Res. A **501**, 499 (2003).
[24] M. Ishii, K. Harada, Y. Hirose, N. Senguttuvan, M. Kobayashi, I. Yamaga, H. Ueno, K. Miwa, F. Shiji, F. Yiting, M. Nikl, and X. Q. Feng, Opt. Mater. (Amsterdam, Neth.) **19**, 201 (2002).
[25] D. P. Bortfeld and M. Meier, J. Appl. Phys. **43**, 5110 (1972).